REPORT DOCUMENTATION PAGE

Form Approved OMB NO. 0704-0188

1. REPORT DATE (DD-MM-YYYY)	2. REPORT TYPE	3. DATES COVERED (From - To)
23 May 2013	Final Report	20 Sep 2010 - 19 Feb 2012

4. TITLE AND SUBTITLE

Turbulence Fine Structure, Intermittency, and Large-Scale Interactions in the StableBoundary Layer and Residual Layer: Correlative High-Resolution Measurements andDirect Numerical Simulations

5a. CONTRACT NUMBER

5b. GRANT NUMBER

W911NF-10-C-0109

5c. PROGRAM ELEMENT NUMBER

611102

6. AUTHORS

D. C. Fritts

5d. PROJECT NUMBER

5e. TASK NUMBER

5f. WORK UNIT NUMBER

7. PERFORMING ORGANIZATION NAMES AND ADDRESSES

Northwest Research Associates, Inc.
NorthWest Research Associates Inc.
4118 148th Ave. NE
Redmond, WA 98052 -5164

8. PERFORMING ORGANIZATION REPORT NUMBER

9. SPONSORING/MONITORING AGENCY NAME(S) AND ADDRESS(ES)

U.S. Army Research Office
P.O. Box 12211
Research Triangle Park, NC 27709-2211

10. SPONSOR/MONITOR'S ACRONYM(S)

ARO

11. SPONSOR/MONITOR'S REPORT NUMBER(S)

56732-EV.1

12. DISTRIBUTION AVAILIBILITY STATEMENT

Approved for public release; distribution is unlimited.

13. SUPPLEMENTARY NOTES

The views, opinions and/or findings contained in this report are those of the author(s) and should not contrued as an official Department of the Army position, policy or decision, unless so designated by other documentation.

14. ABSTRACT

Research focused on the first two of the defined science goals related to characterization and understanding of turbulence sources, instability dynamics, and influences in multi-scale stable boundary layer (SBL) flows. During this time, we achieved major successes in both the numerical and the observational components of this study. The scientific motivations for our overall research program are described in Section 2. Sections 3 and 4 describe in greater detail the results obtained and their implications for SBL dynamics and further research foci.

15. SUBJECT TERMS

rbulence sources, instability dynamics, influences in multi-scale stable boundary layer (SBL) flows

16. SECURITY CLASSIFICATION OF:			17. LIMITATION OF ABSTRACT	15. NUMBER OF PAGES	19a. NAME OF RESPONSIBLE PERSON
a. REPORT	b. ABSTRACT	c. THIS PAGE			David Fritts
UU	UU	UU	UU		19b. TELEPHONE NUMBER: 303-415-9701

Report Title

Turbulence Fine Structure, Intermittency, and Large-Scale Interactions in the StableBoundary Layer and Residual Layer: Correlative High-Resolution Measurements andDirect Numerical Simulations

ABSTRACT

Research focused on the first two of the defined science goals related to characterization and understanding of turbulence sources, instability dynamics, and influences in multi-scale stable boundary layer (SBL) flows. During this time, we achieved major successes in both the numerical and the observational components of this study. The scientific motivations for our overall research program are described in Section 2. Sections 3 and 4 describe in greater detail the results obtained and their implications for SBL dynamics and further research foci.

Final Report for ARO Contract W911NF-10-C-0109

"Turbulence Fine Structure, Intermittency, and Large-Scale Interactions in the Stable Boundary Layer and Residual Layer: Correlative High-Resolution Measurements and Direct Numerical Simulations"

PI: D. C. Fritts

Date**:** 5 April 2012

Period of Performance: 20 September 2010 to 19 February 2012

1. Overview

This report describes research performed under the ARO contract cited above during its first 17 months. The contract was terminated early in order to migrate the funding elsewhere.

Our efforts during this first ~40% of the proposed research focused on the first two of the defined science goals related to characterization and understanding of turbulence sources, instability dynamics, and influences in multi-scale stable boundary layer (SBL) flows. During this time, we achieved major successes in both the numerical and the observational components of this study. The scientific motivations for our overall research program are described in Section 2. Sections 3 and 4 describe in greater detail the results obtained and their implications for SBL dynamics and further research foci.

2. Science Motivation and Goals

Measurements performed during the CASES-99 field program and more recently demonstrated that the stable boundary layer (***SBL***) and the residual layer (***RL***) exhibit a wide range of dynamics on multiple scales. In particular, very high-resolution vertical profiling of winds and temperature has revealed that small-scale structure and turbulence are virtually always present. The sources and persistence of turbulence in stable or very stable atmospheric boundary layers have proven challenging to characterize because of the small scales and the very high-precision measurements required. Yet they are also critical to an improved understanding of SBL dynamics and their implications for transport of heat, momentum, and constituents, dispersion of plumes or contaminants, and the parameterization of these processes in large-scale, mesoscale, and numerical weather prediction (***NWP***) models, to cite a few examples.

Understanding state-of-the-art measurements in the SBL and RL is challenging because single-point measurements of any type often cannot distinguish spatial and temporal variations. Even with multiple such measurements, it is difficult to define all of the relevant spatial and temporal scales, to characterize the larger-scale environment fully, and to interpret observations unambiguously. But with multiple such measurements, coupled with suitable models of these SBL and RL dynamics providing a context within which to interpret the measurements, significant advances in understanding SBL and RL dynamics, mixing, and transport are likely. Indeed, there is considerable synergism between 1) measurements able to define SBL and RL temperature, wind, and turbulence profiles with high resolution and precision at multiple sites and 2) high-resolution direct numerical simulations (***DNS***) able to describe the larger-scale dynamics and their implications for instability and turbulence at smaller scales. This synergism provides a unique opportunity to advance our understanding of SBL and RL dynamics.

Specific goals of our SBL and RL research employing our combined measurement and modeling capabilities included the following:

1) characterization of the tendency for instability and turbulence in general multi-scale SBL and RL flows, and their respective time scales,

2) understanding the instability dynamics that drive large- and small-scale turbulence, their scales, and their dependence on multi-scale environmental parameters,

3) implications of these instability dynamics for mixing, dispersion, SBL and RL evolution, and subsequent instabilities and turbulence, and

4) testing, and guidance for improving, parameterizations of the effects of these dynamical processes in large-scale models.

3. Research Progress in SBL Measurements

During this research effort, we incorporated numerous design changes, new instrumentation, and telemetry enhancements into our measurement systems. Collectively, these efforts resulted in greatly improved capabilities for high-resolution profiling of the SBL and RL. Improvements in our current airborne platform, the DataHawk (formerly Stryker), have been significant and include:

- Improved attitude and roll stability
- Ground temperature sensor for BL thermal correlations
- accurate in-flight temperature calibration with very linear response (thermistor/cold wire)
- Humidity sensing that works very well
- Completely autonomous operation, launch to landing
- Broadband (cold-wire) turbulence (C_T^2) measurement capability with ~few m resolution
- Extended-range telemetry capability to altitudes of 9 km
- Development of a triple failsafe abort capability for flight safety
- A balloon-launch capability for higher-altitude studies
- Developed a 2-sceen capability for simultaneous flight monitoring & scientific evaluation

Based on these improvements, we progressed significantly and performed several field measurement programs. Following test campaigns in Boulder, we made a series of measurements at the Smoky Hill Air National Guard (ANG) site near Salinas, KS, and at two separate sites in Peru (at no travel costs to this grant). Although additional plans were in place to operate at the Army's Dugway Proving Grounds (DPG) in Nevada, the required supplemental ARO funding was unavailable. As we will discuss briefly below, the Peru site also had a number of significant advantages for possible future expanded operations (see discussion below).

At this stage, the basic operating mode of the DataHawk is to autonomously spiral upwards/downwards in circles (diameters of a few hundred meters) with ascent/descent rates anywhere between ± a few m/s, including flying at a constant height. While other modes are equally possible, the data set from the spiral (helical) modes alone has proven to be more than sufficient for these initial measurements. As mentioned above, launch and landing are autonomous. Launch, which is accomplished using a Bungee-like launch platform, is initiated by computer command via telemetry (2.4 GHz). Because of its Styrofoam construction, pusher propeller, and imbedded instrumentation, the DataHawk is remarkably rugged and can land

virtually anywhere. The normal landing site is near the launch pad. Typical battery life is around 40 minutes, with battery change made easily following landing.

The two flight patterns employed consist of 1) ascending and descending at a constant rate while flying in circles or 2) flying to a specified height(s) and remaining there while making a series of constant altitude circles. As shown below, both modes provide unique data sets.

Two-way telemetry enables both 1) monitoring and modifying the flight plan during the flight, and 2) viewing the down-linked data and flight information 'on-line'. We also improved the telemetry link by incorporating high-gain, circularly-polarized, ground-based antennas. As a result, the DataHawk operating range has been extended to well over 10 km.

Examples of the new measurement capabilities, along with a few tantalizing, albeit preliminary, conclusions are shown in the following paragraphs.

3.1. DataHawk flight modes

Figure 1 shows examples of 1) a constant rate ascent/descent mode and 2) a constant height mode (various heights) that can be pre-programmed or altered during fight. Figure 2 shows a plan view of circular flight patterns. Note the accuracy of the ascent descent mode, the constancy of the fixed height mode, and the repeatability of the circle patterns.

3.2. Examples of DataHawk Measurements

3.2.a. Temperature Profiles

Figure 3 shows an example of a high-resolution temperature profile from the surface to 1300 m. This profile illustrates the steep temperature inversion routinely found at Paracas (see below). Note the maximum height of 1300 m.

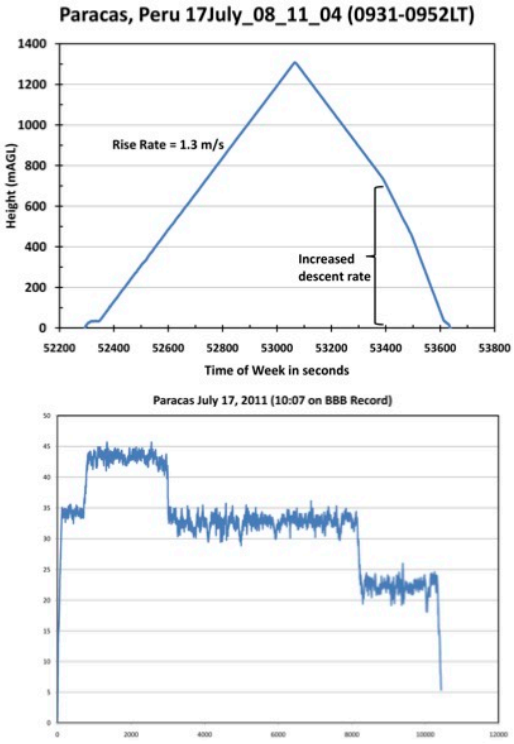

Figure 1. DataHawk profiles showing constant ascent/descent and constant altitude capabilities (top and bottom).

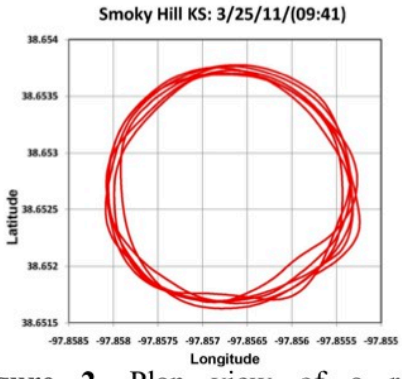

Figure 2. Plan view of a repeated DataHawk circular flight pattern showing the repeatability and stability of the measurement capability.

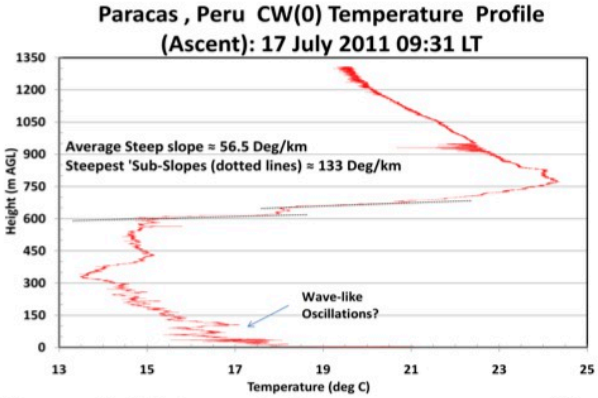

Figure 3. High-resolution temperature profile showing a strong inversion and significant small-scale structures from 0 to ~1300 m.

3.2.b. Wind Measurements

Wind speed and direction determined from ascending helical circles (Figure 4) measured simultaneously with the steep temperature gradient (Figure 3) show pronounced variations in the region of the steep gradient. While these measurements provide reasonable ~100 m resolution of the wind field, we anticipate also developing much higher resolution measurements of horizontal winds during the next year.

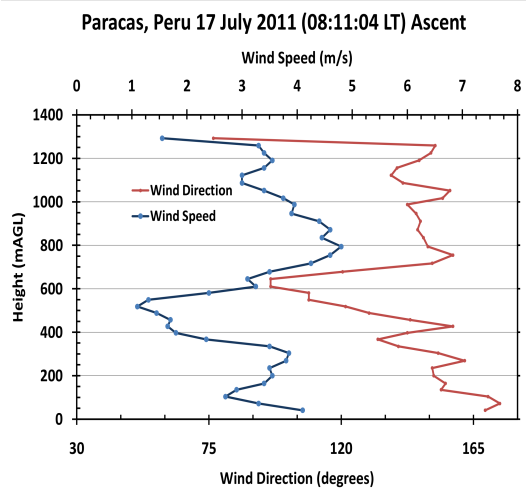

Figure 4. Wind speed (blue) and direction (red) obtained from the DataHawk GPS positioning system computed during circling maneuvers.

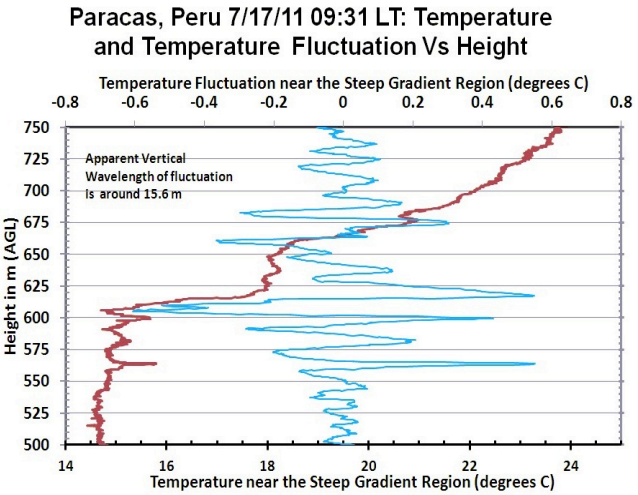

Figure 5. Oscillatory features in the fine-structure temperature field that are indicative of GWs (blue) and the temperature profile in which they occur.

3.2.c Wave-like fluctuations in a steep thermal gradient

Figure 5 illustrates the capability of the DataHawk to resolve gravity wave (***GW***) temperature structures in narrow height ranges. Note the clear periodic nature of the GWs. These features are especially apparent in the steep temperature inversion, with very little evidence for such outside.

3.2.d. Potential high-resolution measurements of C_T^2

Figure 6 shows the first C_T^2 profile obtained during the DataHawk test flights at Paracas, Peru. These reveal the enormous potential for this measurement technique with the high sensitivity to small magnitudes at the higher altitudes.

3.2.e. Potential high-resolution studies of thermals

Figure 7 shows the results of an analysis of high-bandwidth temperature fluctuations made mid-morning at the Smoky Hill site. In this case the DataHawk was flying in constant-height circles in the same location for many tens of minutes. Note the sporadic nature of the

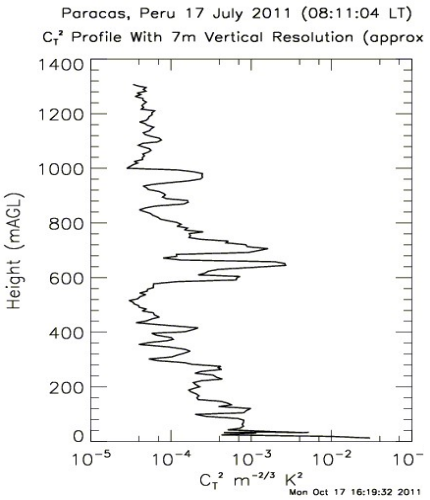

Figure 6. C_T^2 profile obtained from DataHawk temperature measurements for the flight profile shown in Figure 1.

fluctuations. We postulate that these fluctuations are associated with nascent thermals that will ultimately grow into full-scale features, and ultimately produce clouds. The fluctuations were observed at all three locations, and are correlated with enhanced humidity features.

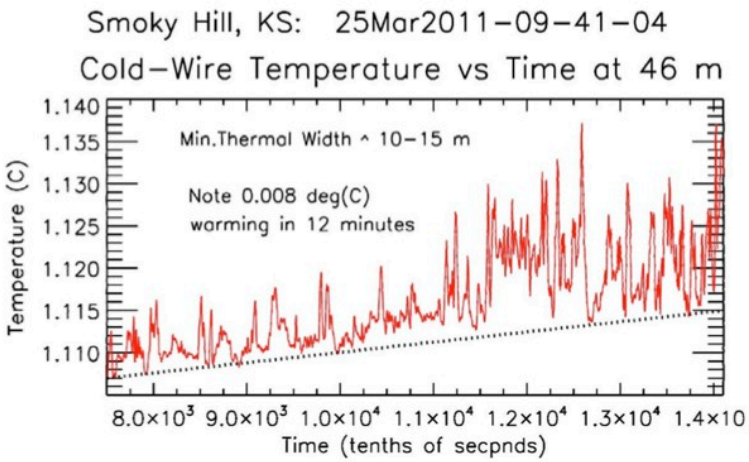

Figure 7. High-bandwidth temperature fluctuations measured by the DataHawk over Smoky Hill KS under daytime convective boundary layer conditions. Note the quasi-periodic temperature enhancements that we believe are evidence of localized convective plumes.

3.3. Discussion of the two Peruvian sites

The two sites used in the Peruvian campaigns were Paracas (a coastal site some 300 km south of Lima), and the Jicamarca Radio Observatory (JRO) located in the Andean foothills. Paracas is essentially an unoccupied desert location, while JRO is the site of a well-known atmosphere-ionosphere observatory containing the world's largest antenna, along with a number of additional atmospheric radars. Relative to existing sites in the U.S., the two Peruvian locations provide significant advantages for the specific SBL and RL studies relevant to our ARO funding. These are listed below.

3.3.a. Paracas

Paracas provides the following attributes and advantages relative to Smoky Hill and/or DPG:

- No site costs (compare with Smoky Hill @ $3k/2 days; DPG @ $10k/campaign)
- Virtually constant acceptable weather conditions (no rain, no storms, no winter)
- Ideal, predictable, perennial wind conditions (minimal nighttime and morning winds)
- Very cooperative, essentially 'on-line', arrangements with the local FAA (CORPAC)
- The existence of a semi-permanent, very steep temperature gradient topping the ABL that arises from the combination of the cold Pacific ocean and the warm tropical atmosphere.

3.3.b. JRO

Advantages for JRO are essentially identical to those for Paracas, except that the temperature gradient is somewhat less steep, and the wind conditions a bit more variable. An additional JRO feature lies with the existence of the radar facility and the associated radar expertise. Moreover, the over-arching Peruvian Geophysical Institute (IGP) now operates a boundary layer radar (BLR) in northern Peru, and we are discussing the possibility of transferring it to JRO specifically for cooperative studies with our DataHawk measurement capabilities.

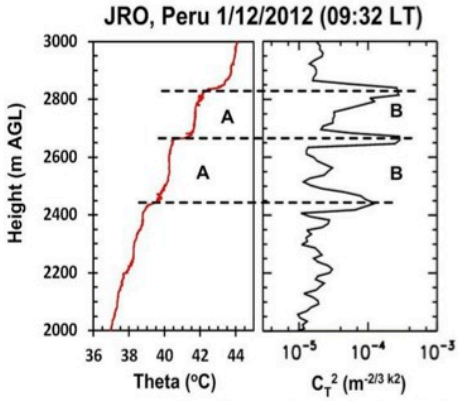

Figure 8. θ (left) and C_T^2 (right) from co-located SOUSY radar and DataHawk measurements at JRO.

With these advantages, and considering the presence of the nearly permanent temperature gradient topping the ABL 24 hr/day, it is clear that Paracas and JRO provide ideal and unique laboratories for ongoing ABL high-resolution research. Data from our most recent measurement program demonstrating the synergism between our *in situ* measurements and the JRO SOUSY radar are shown in Figure 8. These reveal, as seen in other lower-resolution measurements, that T' variance and C_T^2 correlate very well with highly stable, layers rather than the more nearly neutrally-stable layers that appear to have evolved from previous turbulence events.

4. Research Progress in Modeling

4.1. Linear fine structure

We performed an initial suite of DNS of multi-scale interactions that we believe illustrate a range of SBL dynamics containing residual fine structure (***FS***) in the wind field due to previous mixing events and larger-scale gravity waves (***GWs***) which interact and mutually deform each other. Initial studies included two sinusoidal FS shear magnitudes ($\boldsymbol{U_z}$ = d*U*/dz = 2*N* and 1.4*N*, with ***U*** and ***N*** the local FS wind and buoyancy frequency), two FS spatial scales relative to the larger-scale GW (5 and 10 times the GW vertical wavenumber, ***m***), and both streamwise and spanwise (along and across the streamwise plane of GW propagation) FS orientation. These initial studies reveal remarkable sensitivity of SBL large-scale and turbulence evolutions to the details and intensities of the initial flow structures and orientations.

To illustrate the strong influences of FS orientation, we compare in Figure 9 evolutions with streamwise and spanwise FS shears of U_z = 1.4*N*, yielding an initial FS Richardson number of $\boldsymbol{Ri} = N^2/U_z^2 = 0.5$, and a total Ri = 0.125 where the GW with initial amplitude $\boldsymbol{a} = u'/(U\text{-}c) = 0.5$ (with u' and c the GW horizontal perturbation velocity amplitude and horizontal phase speed) induces a weaker stability of *N*/2 in the rising phase of the GW motion. We also choose a Reynolds number of $\boldsymbol{Re} = \lambda_z^2/T_b\nu = 50{,}000$, with $\boldsymbol{\lambda_z} = 2\pi/m_{GW}$ the GW vertical wavelength, $\boldsymbol{T_b} = 2\pi/N$ the buoyancy period, kinematic viscosity $\boldsymbol{\nu}$, and a FS wavenumber of $\boldsymbol{m_{FS}} = 5m_{GW}$.

The two evolutions with larger shears also differ dramatically and provide valuable insights into the dynamics that control SBL

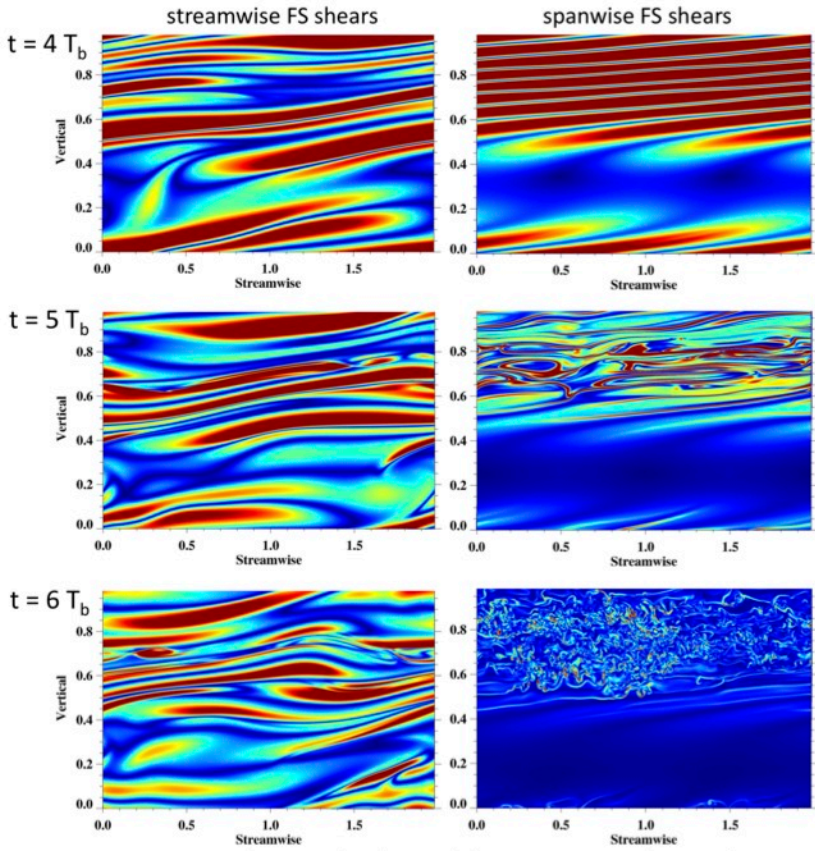

Figure 9. Streamwise-vertical vorticity cross sections of DNS with streamwise and spanwise fine-structure alignments (left and right) at t = 4, 5, and 6 T_b (top to bottom, see text for GW and FS parameters). Note the dramatically different evolutions, with strong large-scale dynamics and weak turbulence at left and weak large-scale dynamics and strong turbulence at right.

evolution in more general flows. The DNS with streamwise FS (Figure 10, bottom panels) is seen to exhibit strong large-scale interactions (with large GW amplitude reductions), but relatively weak and large-scale turbulence that never becomes quasi-isotropic. The DNS with spanwise FS (Figure 10, top panels) is seen instead to exhibit weak large-scale interactions (very weak GW amplitude reductions), but very strong turbulence extending to very small scales. These results suggest that the source of additional quasi-2D large-scale modes in the streamwise FS case is the initial GW-FS interaction, while the source of enhanced turbulence in the spanwise FS case is the initial FS structure itself undergoing deformation by the GW.

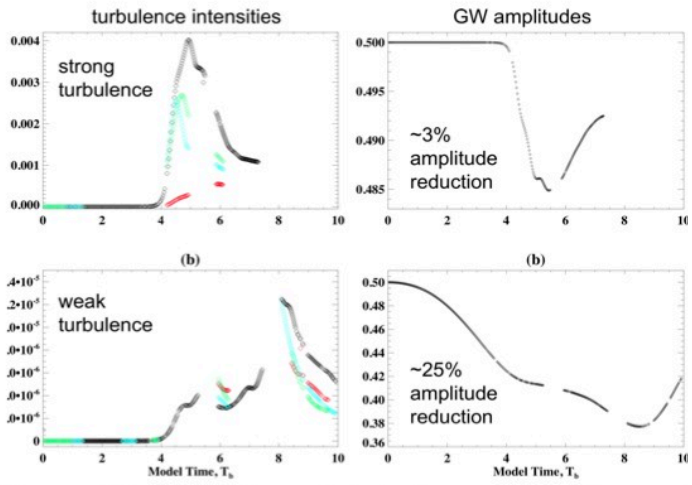

Figure 10. Evolution of turbulence intensities and GW amplitudes (left and right) in the two DNS with spanwise and streamwise FS (top and bottom) displayed in Figure 9.

The reasons for these significant differences in the two flow evolutions can be understood qualitatively by the relative alignments of the FS shears. In the case of streamwise FS alignment (and spanwise FS vorticity, top panel), the large-scale GW contributes only weak additive changes and advection of the FS vorticity. In contrast, spanwise FS (and streamwise FS vorticity) enables the GW to stretch the FS vorticity, thus intensifying FS shears to a much greater degree than for streamwise FS.

When FS shears are stronger, as is often observed, more vigorous instabilities and turbulence events can arise. To examine such influences, two DNS as described above, but with FS shears of $U_z = 2N$, were also performed, and the 2D streamwise-vertical cross sections of the vorticity magnitude fields are displayed at t = 7.5 T_b in Figure 11. These DNS exhibit the same tendencies as discussed above, but now include more intense turbulence in both cases.

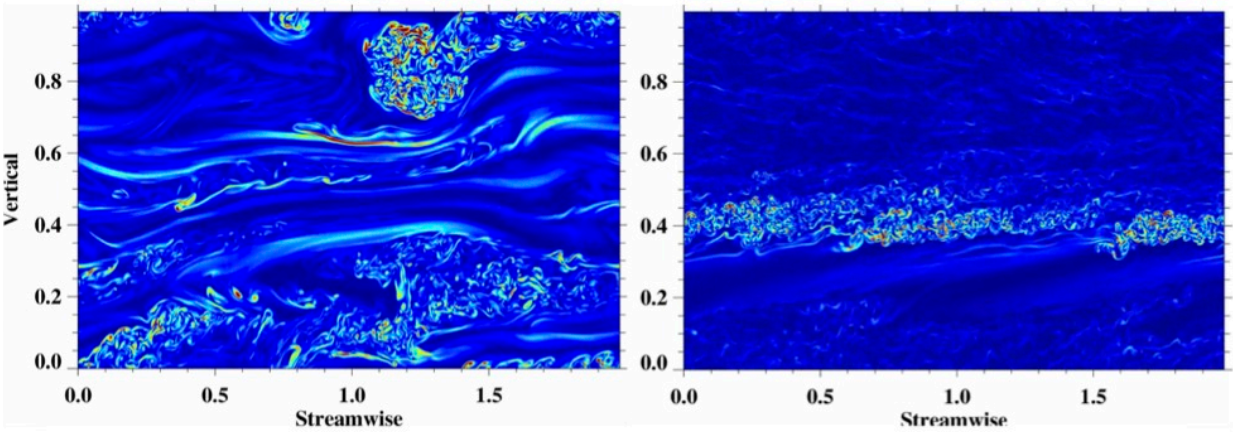

Figure 11. As in Figure 9, but with FS shears of $U_z = 2N$ and t = 7.5 T_b. Note that in the streamwise FS case (left) both large-scale motions and quasi-isotropic turbulence arise from the multi-scale interactions, whereas the spanwise FS case (right) continues to exhibit more intense small-scale turbulence.

We also illustrate the mechanical energy and thermal dissipation rates (ε and X) fields for the DNS shown at left in Figure 11 at t = 5,5, 7.5, 9.5, and 11.5 T_b in Figure 12. The dissipation fields will be especially valuable in comparing with our *in situ* measurements of turbulence parameters in order to constrain our future DNS to observed SBL and RL parameters. Note that the stronger SBL dynamics seen in Figure 12 suggest continuing generation of small-scale

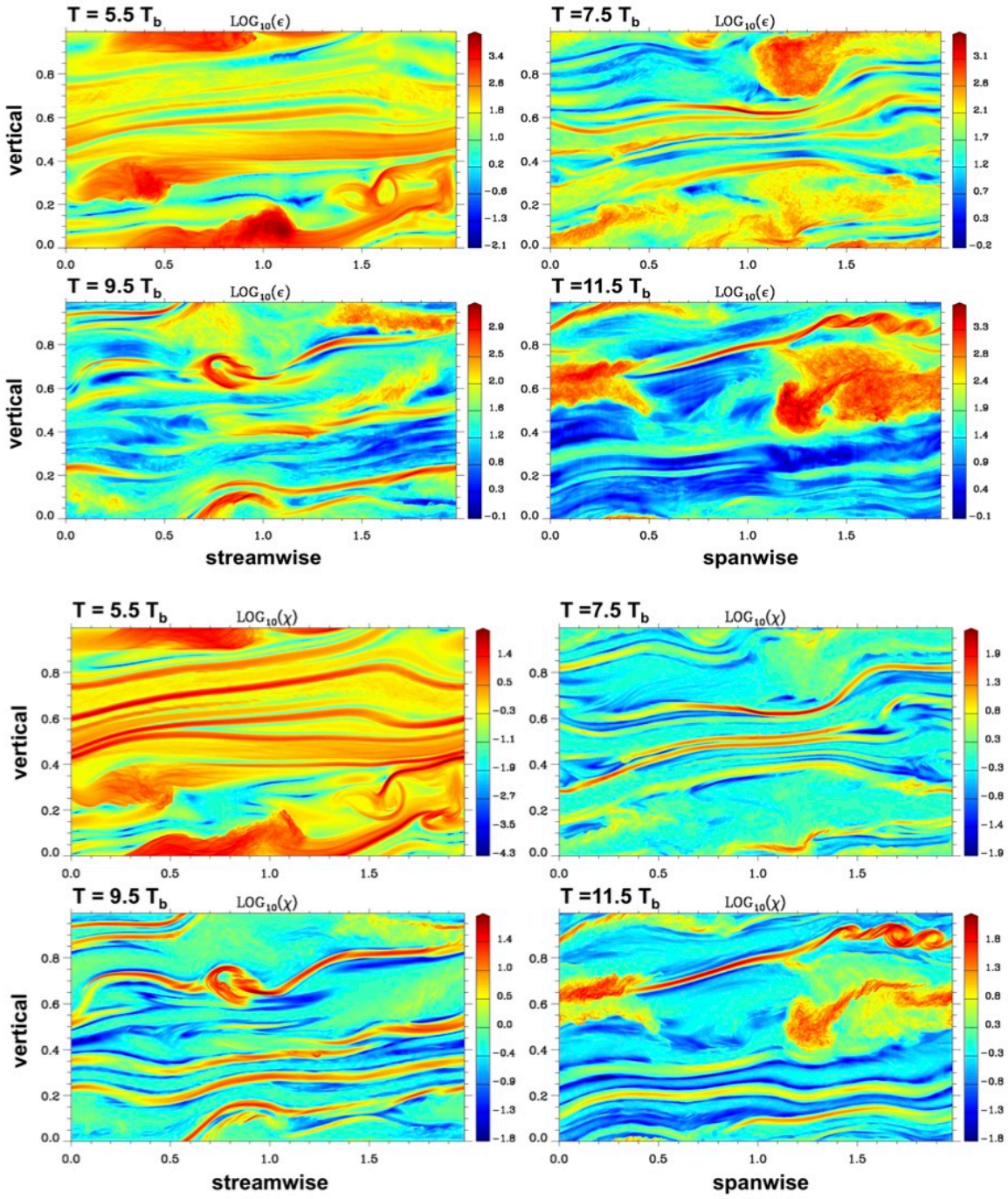

Figure 12. Mechanical energy dissipation rate (ε, top panels) and thermal dissipation rate (X, bottom panels) at t = 5.5, 7.5, 9.5, and 11.5 T_b in the DNS with streamwise FS with shear magnitude $U_z = 2N$. Both fields are shown with log scales.

turbulence throughout the evolution, as is often seen in SBL and RL measurements. There is a strong correlation between strong small-scale vorticity (see the left panel of Figure 11) and large mechanical energy dissipation, as expected in strong turbulence. However, where turbulence mixes the fluid efficiently (and is often most intense) thermal dissipation is weak (compare the upper and lower panels of Figure 12). This has important implications for measurements addressing temperature FS and estimates of turbulence intensities. It also makes high sensitivity especially important in these measurements. In general applications, lack of sensitivity to temperature FS can cause large errors in assessing these dynamics with both *in situ* and radar measurements.

Related simulations, but for somewhat weaker FS shears were also performed and were found, as expected, to yield weaker instability events that contributed much less vigorously to the overall dynamics. In these cases, it appears that significantly larger *Re* would be needed to trigger significant turbulence FS at even smaller scales.

4.2. Rotary fine structure

While we learned a great deal about the competitive tendencies between instability and nonlinear wave-wave interactions in our initial multi-scale simulations having linear FS shears, such shears throughout the atmosphere are very often associated with inertia-gravity waves (IGWs) that have a rotary velocity structure in which the horizontal velocities describe an ellipse (in time and space) with the major axis along the direction of propagation and a corresponding temperature perturbation in phase or anti-phase with the smaller velocity component.

Given this, our next steps towards realism in our numerical studies were to perform four additional simulations having differing IGW major shear magnitudes and orthogonal major-axis alignments. In each case, we chose the larger major-axis shear to be the same as for the results displayed in Figures 9 to 12 above.

These revealed additional interesting, and very surprising, results. Because we had increased overall FS shear variance relative to either of the simulations discussed at length above, we had anticipated that the tendency towards instability at the smallest scales would be even further accelerated. What was found was exactly the opposite. Our initial conclusion was that the rotary nature of the FS shear actually suppressed the dominant previous instability, yielding a later, but then stronger turbulence transition once it was initiated. This will need to be confirmed with a more detailed stability analysis, but the differing results are apparent in Figure 13, which shows the two previous linear FS results discussed above (with spanwise and streamwise FS shears at left and right) and the rotary FS case having equal component FS shears in the center column.

Referring to Figure 13, we note the following:

1. the rotary case exhibits delayed instability dynamics compared to either linear FS case, despite its larger reservoir of FS shear variance (by 2 times),
2. the larger-scale dynamics appear very similar between the rotary and streamwise FS cases through the two evolutions, apparently exhibiting similar wave-wave interactions,
3. the rotary FS shear case appears to exhibit somewhat stronger turbulence at intermediate stages (t = 9 and 10.5 T_b) than the streamwise linear FS case,
4. the rotary and streamwise linear FS cases exhibit an approximate convergence of larger-scale dynamics and turbulence occurrence at later times, and
5. neither the rotary nor the streamwise FS shear cases exhibit any remote similarity to the spanwise FS shear case, despite the much stronger spanwise FS shear dynamics seen to occur when only this FS component was possible (left column of Figure 13).

To explore these differences in another manner, we display the evolutions of the initial GW amplitudes and the total turbulence energies for these three cases in Figure 14. These reveal clear

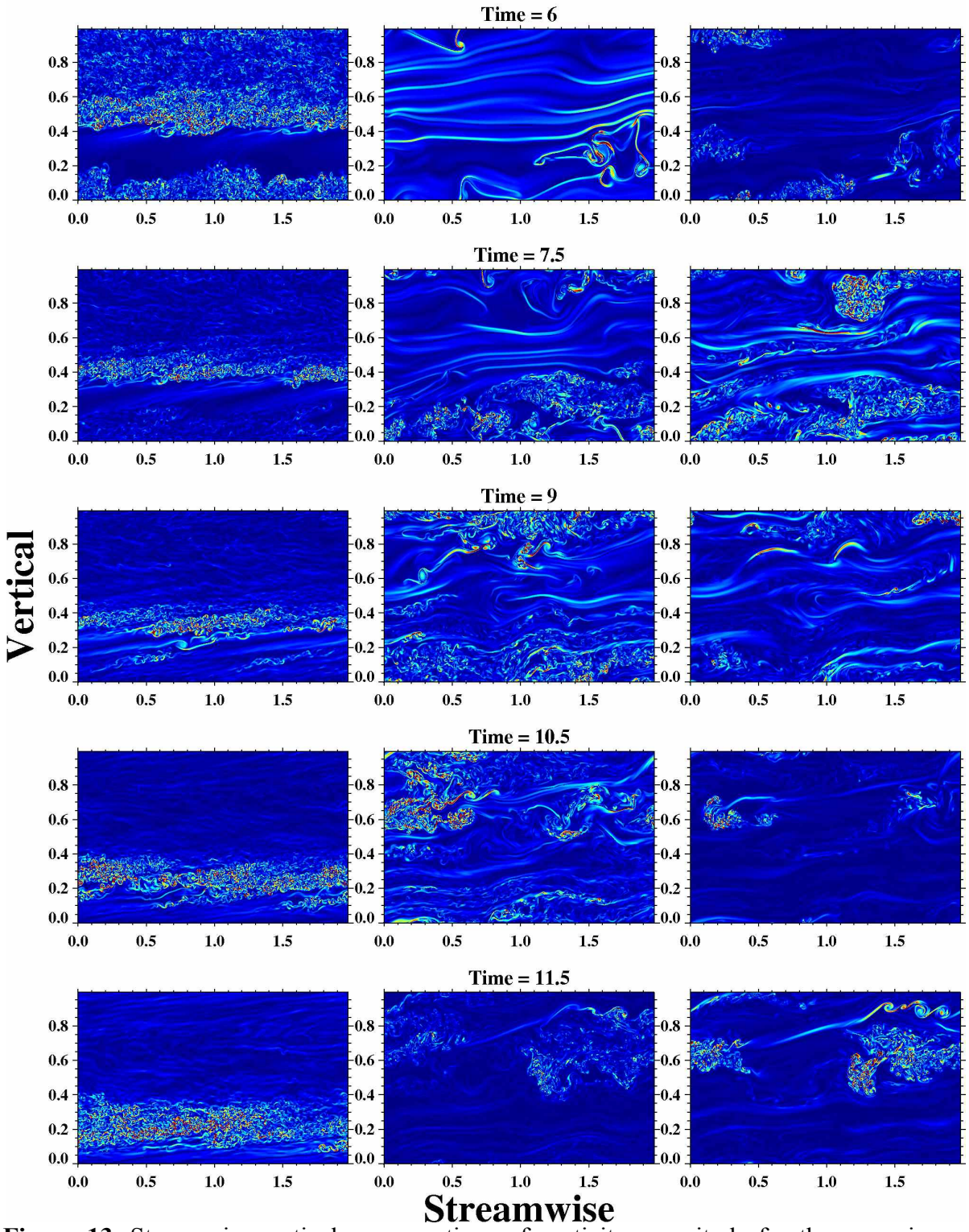

Figure 13. Streamwise-vertical cross sections of vorticity magnitude for the spanwise and streamwise (left and right) linear FS and the rotary FS having uniform shears (center) all with $U_z = 2N$ at t = 6, 7.5, 9, 10.5, and 11.5 T_b. Note that the rotary shear case (center) much more closely resembles the linear streamwise FS shear case (at right), despite equal orthogonal FS shears itself.

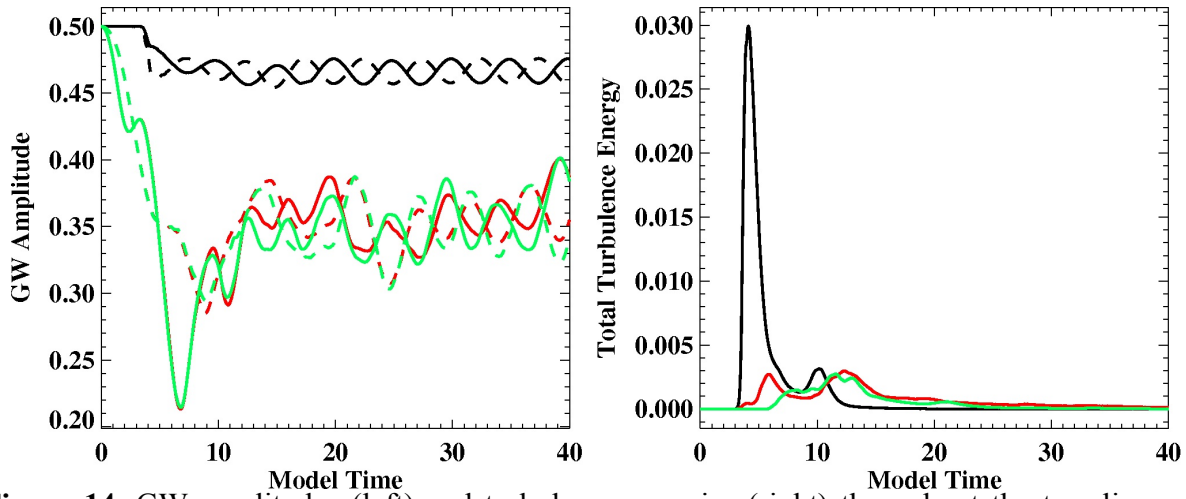

Figure 14. GW amplitudes (left) and turbulence energies (right) throughout the two linear FS shear simulations (black and red for spanwise and streamwise FS shears, respectively), and the rotary shear case (green) from t = 0 to 40 T_b. The rotary case resembles the streamwise FS shear case much more closely, and both depart dramatically from the spanwise FS shear case. Solid and dashed lines at left denote horizontal velocity and temperature amplitudes, respectively.

similarities between the rotary and streamwise linear FS shear cases (red and green, respectively), and their obvious departures from the spanwise FS shear case (black). The former two exhibit relatively dramatic initial GW amplitude decreases accompanying strong wave-wave interactions that account for the streamwise modulation of the vorticity fields shown in Figure 13, especially at intermediate times (~30%, implying a loss of ~50% of the initial GW energy). The case with spanwise linear FS shear, in contrast, exhibits a very small GW amplitude decrease, but dramatically larger turbulence energies. Together, these results establish clearly that multi-scale interactions depend critically on the details of the superposed flows.

5. Research Progress Comparing Measurements and Modeling

The major opportunity for quantitative comparisons of measurements and modeling results in the research described here was through energy dissipation statistics, for which theory predicts log-normal distributions for epsilon arising from stationary, homogeneous, isotropic turbulence. This proved to be very promising, with both measurements and modeling exhibiting apparent superposed log-normal distributions having differing means and widths that evolve separately in time. A few examples of these statistics measured during CASES-99 with the TLS are shown in Figure 15. Note the multiple peaks in most panels suggestive of separate turbulence "events" within these data sets.

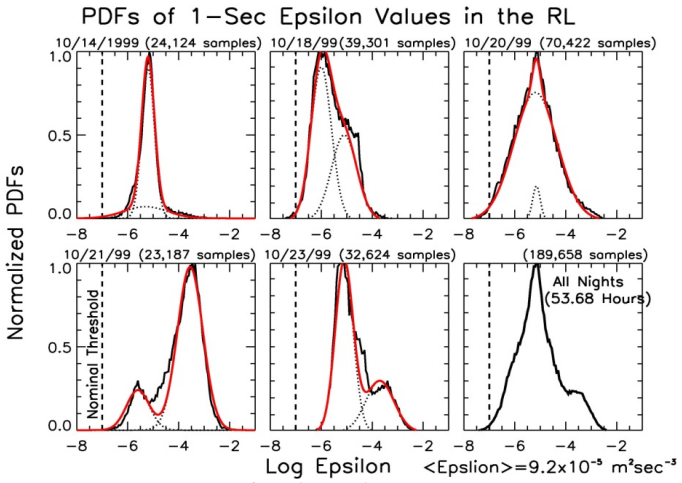

Figure 15. PDFs of ε based on 1-sec measurements aboard the TLS in the residual layer during the CASES-99 experiment. Note the apparent superposition of several or multiple quasi-log-normal distributions at most times.

Similar ε distributions are observed in our DNS studies. Examples from the simulation shown at top in Figure 12 and at right in Figure 13 are displayed in Figure 16 for subsets comprising 1/10th of the vertical domain at times spanning those shown in Figure 13 separated by 1 T_b. As in the observations, there are many cases in which there appear to be multiple peaks, which we anticipate are signatures of separate events.

While in its infancy, we are excited about the prospects for more quantitative studies going forward and expect that such studies will yield significant insights. To facilitate that further, we have enabled a particle-tracking capability in the DNS code that will enable use to "seed" specific events at their onset and observe both the dispersion of individual events and the evolutions of the dissipation fields with time.

6. Publications Submitted and/or in Preparation based on this Research

Balsley, B. B., D. A. Lawrence, R. F. Woodman, and D. C. Fritts, 2012: Fine-scale characteristics of temperature, wind, and turbulence in the lower atmosphere (0-1300 m) over the south Peruvian coast, Bound. Layer. Meteorol., submitted.

Fritts, D. C., L. Wang, and J. Werne, 2012a: GW-fine structure interactions, I: Instability dynamics and competition among instability pathways, J. Atmos. Sci., in preparation.

Fritts, D. C., L. Wang, and J. Werne, 2012b: GW-fine structure interactions, II: Dissipation field evolutions and statistics, J. Atmos. Sci., in preparation.

Fritts, D. C., B. B. Balsley, L. Wang, and J. Werne, 2012c: GW-fine structure interactions, III: Comparisons of dissipation distributions between measurements and modeling, J. Atmos. Sci., in preparation.

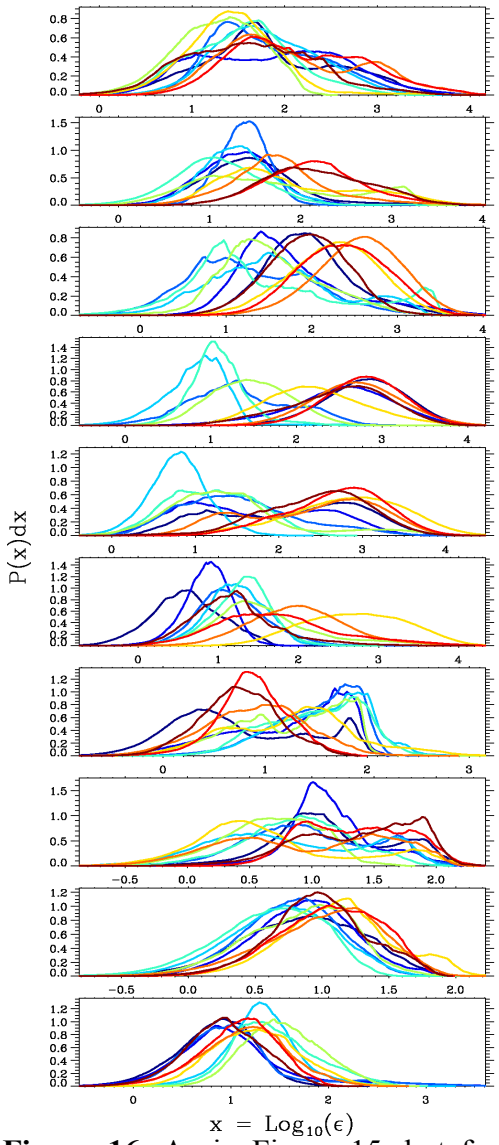

Figure 16. As in Figure 15, but for the simulation shown in the upper panels of Figure 12 and the right panels of Figure 13. Panels top to bottom are from the upper to the lower boundary averaged over 1/10th of the vertical domain. Colors (yellow to blue) show times separated by 1 T_b.

7. Summary

Our research under this ARO funding has enabled major advances in our understanding of SBL dynamics and turbulence statistics, from both measurement and modeling perspectives. It has specifically addressed the implications of multi-scale interactions, their diversity, and their dependence on initial conditions; it has contributed entirely new measurement capabilities for critical SBL flow characterization; it has demonstrated dramatic, new numerical simulation capabilities, and it has provided tantalizing indications that we are able to measure and model the same phenomena, specifically individual turbulence events at high *Re* and the dissipation statistics of various levels of SBL turbulence. All of these suggest a potential for very fertile research in these areas in the future.